Molecular Crystals and Liquid Crystals Science and Technology. Section A. Molecular Crystals and Liquid Crystals

Publication details, including instructions for authors and subscription information:
http://www.tandfonline.com/loi/gmcl19

Crystal Structure and Empirical Calculations for a Chiral Smectogenic Compound with an Antiferroelectric Arrangement

Michel Laguerre [a], Isabelle Zareba [b], Hassan Allouchi [b], Huu Tinh Nguyen [a] & Michel Cotrait [b]

[a] Centre de Recherche Paul Pascal, Avenue A. Schweitzer, 33600, PESSAC, France

[b] Laboratoire de Cristallographie et Physique Cristalline, Universite Bordeaux I, 351 Cows de la Libération, 33405, TALENCE Cédex, France

Version of record first published: 04 Oct 2006

Mol. Cryst. Liq. Cryst., Vol. 317, pp. 165–180
Reprints available directly from the publisher
Photocopying permitted by license only

Crystal Structure and Empirical Calculations for a Chiral Smectogenic Compound with an Antiferroelectric Arrangement

MICHEL LAGUERRE[a], ISABELLE ZAREBA[b], HASSAN ALLOUCHI[b], HUU TINH NGUYEN[a] and MICHEL COTRAIT[b,*]

[a] *Centre de Recherche Paul Pascal, Avenue A. Schweitzer 33600 PESSAC, France;*
[b] *Laboratoire de Cristallographie et Physique Cristalline, Université Bordeaux I, 351 Cours de la Libération, 33405 TALENCE Cédex, France*

(Received 3 October 1997; In final form 28 January 1998)

This paper relates a comparative study of crystal structures of two isomeric compounds. They differ only through their polyaromatic group sequence: O—Ø—CO_2—Ø—C≡C—Ø—CO_2 on the one hand and O—Ø—C≡C—Ø—CO_2—Ø—CO_2 on the other, and give rise to very different polymorphisms. The chiral mesogenic (S) 1-methylheptyl 4-[(4-octyloxy-3-fluoro) benzoyloxy]tolan-4′ carboxylate (8FBTO1M7) crystallizes in the $P2_12_12_1$ space group, with two different molecules **A** and **B** per asymmetric unit ($Z = 8$) with $a = 7.903(2)$, $b = 11.324(1)$ and $c = 80.576(6)$ Å. The polyaromatic central cores of both molecules are parallel and aligned in the same direction, giving dimers with a tilt angle close to 11°. The molecules give rise to sheets, of which the arrangement is smectic C and is antiferroelectric-like. The repetitive unit in the crystal phase is a bilayer one, where molecules are alternatively tilted from one layer to the other. The molecular arrangement is compared with that of the (S) 4-[1-methylheptyloxy-carbonyl]phenyl 4-heptyloxytolan-4′ carboxylate (7TBO1M7) which gives rise to a very rich polymorphism, including ferro-, antiferro- and ferri-electric phases. The binding energy within a sheet and between neighbouring sheets was evaluated by using molecular mechanics for both compounds. It seems that the relative positions of the benzyl and tolan groups inserted between the polar ester and ether groups in the polyaromatic central core, is of a prime importance in the molecular arrangement and consequently in the mesomorphic sequence.

Keywords: Chiral mesogenic compounds; antiferroelectric mesogens; crystal structure; theoretical calculations

*Corresponding author.

1. INTRODUCTION

A good correlation has generally been found between the crystal structure and the mesomorphic behaviour of a great number of non-chiral mesogenic compounds [1, 2] and more recently in a few chiral smectogenic compounds [3–9]. For the latter, the smectic C-like arrangement in the crystal is in agreement with the transition to an S_C^* phase.

This is also the case for a few compounds exhibiting ferro-, antiferro- and ferri-electric properties [10–12], particularly for the well-known MHPOBC* molecule [10] whose structure with an alternate arrangement of the highly polar layers was interpreted to be responsible for the antiferroelectricity in the liquid crystalline phase. Moreover, for the latter, a peculiar structural feature has been described: the chiral alkyl chains are almost perpendicular to the core moiety [10, 11] and face each other between neighbouring layers. Such an arrangement has been observed in the crystal structure of the chiral mesogenic compound (S) 4-[1-methylheptyloxycarbonyl]phenyl 4-heptyloxytolan-4′ carboxylate (7TBO1M7) showing a very rich polymorphism [13].

It is now well established that the local dipolar moments in the molecular structure of thermotropic liquid crystals play an important role in the appearance of such mesophases, and are at the origin of different molecular interactions.

The following three series:

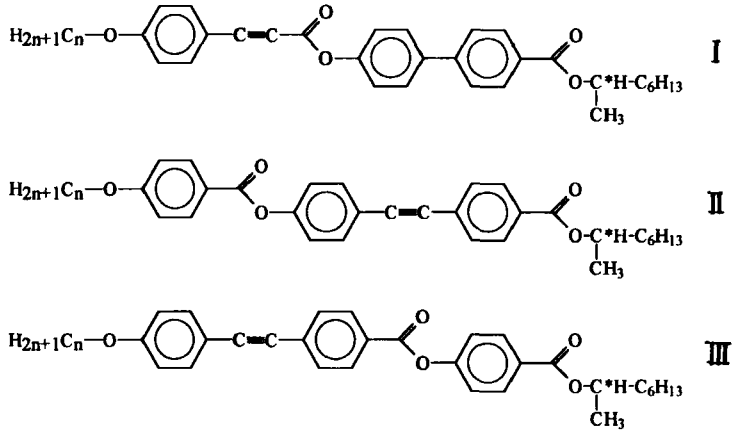

* 4(S)-[1-methylheptyloxycarbonyl]phenyl 4-octyloxbiphenyl-4′-carboxylate.

with similar alkoxy and chiral alkyl chains and isomeric central polyaromatic cores with the same length exhibit different mesomorphic sequences because their local dipolar moments are arranged differently.

Series I displays the twist grain boundary smectic A (TGB_A phase) with cholesteric textures. With series II, we observed only S_C^* and S_A or S_C^* and TGB_A phases with filament textures, depending on the length of the alkoxy chain, but we could not determine its helical pitch [15]. On the other hand, series III exhibits a totally different mesomorphic sequence with ferro-, antiferro- and ferri-electric smectic phases [16]. The crystal structure of $7TBO_1M_7$ (series III with $n = 7$) has been solved as stated above [13].

To investigate the role of the relative positions of the polar groups in the polyaromatic central core on the polymorphism of the mesophase, we determined the crystal structure of a series II compound exhibiting only the S_A phase (with $n = 8$ and a fluorine atom branched on the first cycle), the (S)-1-methylheptyl 4-[(4-octyloxy-3-fluoro)benzoyloxy]tolan-4′carboxylate (8FTBO1M7). The compound analogous to 8FBTO1M7 but without fluorine did not give good enough crystals. The crystal structures of both compounds were completed with theoretical calculations of the dipolar moments and binding energies to obtain a better understanding of their molecular arrangement, thus leading to their different mesomorphic sequences.

2. EXPERIMENTAL

2.1. Crystal Structure

2.1.1. Crystal Data and X-ray Measurements

Colourless crystals of $8FBTO_1M_7$ were grown by evaporation from ethanol/chloroform solutions. They were fragile, soft and often twinned. The crystal used for the X-ray measurements was lamellar, with dimensions $0.05 \times 0.3 \times 0.6$ mm. The unit-cell parameters were obtained by a least-squares fit of the setting angles of 25 reflections with θ between 18° and 39°. The crystal data are given in Table I.

TABLE I Crystal data

Formula	$C_{38}H_{45}O_5F$	a(Å)	7.903(2)
Mx(g mole^{-1})	600.8	b(Å)	11.324(1)
System	Orthorhombic	c(Å)	80.576(6)
Space group	$P2_12_12_1$	v(Å^3)	7211
Z	8	Dx(g cm^{-3})	1.107
F(000)e$^-$.cell^{-1}	2576	μ(CuKα) mm^{-1}	0.617

The diffracted intensities were collected on a CAD-4 Enraf-Nonius diffractometer for the monochromatized CuKα radiation (λ = 1.54178 Å) with θ_{max} = 50° and $0 \leq h \leq 7$, $0 \leq k \leq 11$, $0 \leq l \leq 80$ using the ω-2θ scan mode. There were 4297 reflections collected, of which 3754 were unique (R_{int} = 0.021); only 2090 reflections were considered as observed ($I > 2\sigma(I)$). Experimental absorption correction was performed using the Ψ scan technique [17]. The minimum and maximum absorption factors were T_{min} = 0.85 and T_{max} = 0.99. Three standard reflections were used and measured every two hours; there was no decrease in intensity during data collection.

2.1.2. Structure Determination and Refinement

The crystal structure was solved using both the Mithril [18] and the Shelx86 [19] packages, which allowed location of two-thirds of the non-hydrogen atoms. The remaining ones were positioned through several successive Fourier syntheses. Refinement was performed thanks to the Shelx76 program [20], using constraints on several bond lengths and angles. The hydrogen atoms were introduced at their theoretical positions and allowed to ride with the carbon atoms to which they were attached. Refinement was performed on F with the following weighting scheme $w = 3.122/(\sigma(F)^2 + 0.00545F^2)$. The final reliability factors were $R = 0.114$ and $wR = 0.115$. These high values can be related to the rather high thermal motion U_{eq} factors and probably to some disorder.

2.2. Theoretical Calculations

The partial punctual electronic charges and the dipolar moments were calculated with the MOPAC 6.0 package, using the MNDO method.

The calculations were performed on a SGI Indy R4400 Silicon Graphics station, using Insight II and Discover 95.0 packages. The binding energies were evaluated using molecular mechanics, with the CVFF (Consistent Valence Force Field) method [21].

The starting conformations were those found in the crystal structure for both compounds. As we had already observed, preliminary attempts showed that gradient conjugate minimization methods led to a large distorsion of the crystalline conformation of an isolated molecule. In the present case where it is essential to preserve the crystalline conformation, the best minimization method is the steepest descent (SD). This procedure was

performed without any distance cutoff* (the electrostatic interactions are significant even at a large distance) until the energy variation was less than 0.02 kcal/cycle (3000 cycles); the root mean square (RMS) was less than 0.3 Å at the end of the calculation.

3. RESULTS AND DISCUSSION

3.1. X-ray Structure Analysis

Atomic parameters (x, y, z and U_{eq}) are given in Table II. Note the very high values of several U_{eq} factors, most of which belong to the COO—C*H (CH_3)—C_6H_{13} and OC_8H_{17} terminal chains. The U_{eq} atomic factors of the terminal chains increase from the beginning to the end of such chains, as observed in other mesogenic structures [22, 23]. This is in agreement with the rather low density ($D_X = 1.107\,g\,cm^{-3}$) observed.

For the sake of clarity, only the stick-and-ball representation of both independent molecules **A** and **B** with atom labelling is presented in Figure 1.

To simplify the comparison between the two independent molecules **A** and **B**, the atomic numbering runs from C1 to C43 for molecule **A** and from C51 to C93 for molecule **B**. Bond lengths are given in Table III with their standard deviations in brackets; a few of the latter are large and explain some rather large discrepancies of bond lengths with those observed in the well-defined $7TBO_1M_7$ structure [13]. To allow an easy comparison of bond lengths in molecules **A** and **B**, the equivalent atoms were named identically; C1 to C43 as far as the molecule **B** is concerned stand for C51 to C93.

3.1.1. Molecular Conformations

The two cristallographically independent molecules are not fully extended. The lengths of molecules **A** and **B** (distance between the terminal carbon atoms) are respectively equal to 34.90(3) and 35.78(3) Å, compared with the length of the molecule in its most extended form** close to 44 Å. The (C43...C*27...C34) and (C93...C*77...C84) angles are respectively close to 128° and 146° for molecules **A** and **B**.

*The cutoff distance is the interatomic distance above which the calculations are not performed.

**Calculated from a CPK model.

TABLE II Fractional coordinates ($\times 10^4$) and equivalent isotropic thermal parameters $U_{eq}(\text{Å}^2) = 1/3 \sum_i \sum_j u_{ij} a_i^* a_j^* \mathbf{a}_i.\mathbf{a}_j$

	x/a	y/b	z/c	U/U_{eq}
C1	5600(26)	1458(24)	2939(2)	86(25)
C2	5955(20)	2327(17)	2821(2)	63(22)
C3	5712(18)	2134(11)	2658(2)	25(17)
C4	4901(25)	1157(12)	2610(3)	69(23)
C5	4271(23)	302(15)	2710(2)	54(20)
C6	4682(23)	539(16)	2875(4)	75(24)
F106	4315(14)	−200(8)	3002(2)	94(14)
C7	4416(19)	895(14)	2434(2)	28(18)
O8	4916(16)	1785(8)	2340(2)	60(14)
O9	3552(17)	93(10)	2392(1)	69(15)
C10	4616(20)	1647(14)	2157(2)	39(19)
C11	3607(27)	2442(18)	2091(3)	77(24)
C12	3165(20)	2348(16)	1920(3)	55(20)
C13	3773(23)	1522(16)	1818(3)	65(23)
C14	4952(23)	737(17)	1883(3)	64(22)
C15	5309(26)	731(16)	2060(3)	74(23)
C16	3294(34)	1448(21)	1652(4)	93(27)
C17	3059(24)	1276(20)	1512(4)	81(25)
C18	1360(34)	1061(28)	830(3)	141(32)
O19	718(28)	2038(24)	748(2)	207(29)
C20	2581(24)	1354(21)	1341(3)	72(25)
C21	1910(35)	2328(20)	1264(3)	127(28)
C22	1603(33)	2149(30)	1099(3)	147(32)
C23	1709(35)	1044(28)	1019(3)	125(30)
C24	2633(30)	217(20)	1115(3)	142(30)
C25	3024(28)	283(30)	1280(3)	118(28)
O26	1551(40)	83(19)	758(3)	258(31)
C27	−143(24)	1949(21)	594(3)	249(36)
C28	1467(24)	2192(30)	496(3)	290(38)
C29	−1262(24)	2973(21)	559(3)	273(36)
C30	−2768(35)	2832(26)	452(5)	477(42)
C31	−3505(55)	4063(25)	417(3)	371(40)
C32	−3900(50)	4238(24)	237(4)	402(41)
C33	−4034(42)	5517(29)	186(5)	510(42)
C34	−5841(41)	5978(30)	195(5)	483(41)
O35	5798(13)	1666(8)	3109(1)	60(12)
C36	6854(23)	2680(13)	3155(2)	72(21)
C37	6887(26)	2574(18)	3341(2)	120(26)
C38	7796(31)	1603(23)	3433(3)	215(33)
C39	7299(37)	1730(35)	3618(3)	300(37)
C40	8821(30)	1420(24)	3713(3)	185(31)
C41	9083(35)	1607(33)	3893(3)	255(35)
C42	10340(61)	963(41)	3983(4)	462(42)
C43	10313(49)	1199(33)	4170(3)	417(41)
C51	10596(18)	−1154(11)	2952(2)	39(17)
C52	11019(26)	−2013(17)	2838(2)	93(24)
C53	10615(35)	−1894(16)	2671(3)	167(30)
C54	9733(30)	−887(21)	2626(2)	93(25)
C55	9444(30)	52(16)	2735(3)	124(27)
F156	9270(15)	618(8)	3009(1)	97(14)
C56	9867(26)	−140(14)	2895(2)	81(23)
C57	9338(25)	−581(20)	2443(3)	95(27)

TABLE II (Continued)

	x/a	y/b	z/c	U/U_{eq}
O58	9932(19)	−1354(12)	2327(1)	76(17)
O59	8602(24)	263(10)	2386(2)	130(21)
C60	9557(27)	−1344(15)	2170(4)	92(26)
C61	8490(23)	−2101(16)	2097(3)	68(22)
C62	8059(28)	−1994(16)	1926(4)	96(26)
C63	8972(27)	−1130(17)	1846(2)	73(24)
C64	9956(25)	−320(13)	1923(3)	86(24)
C65	10295(29)	−411(22)	2088(3)	104(27)
C66	8573(33)	−1028(23)	1664(5)	123(30)
C67	8154(37)	−969(20)	1521(5)	113(29)
C68	6346(55)	−219(28)	817(4)	229(38)
O69	6175(34)	−1351(23)	755(2)	255(31)
C70	7760(34)	−941(22)	1332(4)	156(32)
C71	6793(31)	−1788(20)	1252(3)	117(29)
C72	6352(39)	−1719(23)	1078(3)	142(30)
C73	6574(36)	−632(25)	996(4)	131(31)
C74	7399(36)	265(28)	1082(2)	176(32)
C75	8047(35)	111(22)	1243(3)	185(35)
O76	6550(38)	662(22)	758(3)	252(32)
C77	5996(29)	−1397(35)	584(3)	305(41)
C78	7662(36)	−1508(38)	487(4)	360(41)
C79	4340(26)	−2090(25)	569(3)	280(35)
C80	3830(31)	−2132(32)	386(3)	285(38)
C81	2082(37)	−2653(33)	388(3)	438(40)
C82	1067(40)	−2338(27)	236(4)	408(41)
C83	419(57)	−3436(30)	149(4)	374(41)
C84	−278(57)	−3164(37)	−21(4)	511(42)
O85	10875(14)	−1273(9)	3114(1)	66(13)
C86	11824(22)	−2306(14)	3174(2)	115(24)
C87	11793(34)	−2150(20)	3357(2)	188(32)
C88	12787(36)	−1134(19)	3425(2)	177(31)
C89	13245(39)	−1318(24)	3607(3)	299(36)
C90	13858(45)	−252(26)	3693(3)	408(41)
C91	13596(41)	−227(26)	3877(3)	326(37)
C92	14517(49)	−1120(30)	3974(3)	348(39)
C93	15001(38)	−664(24)	4144(3)	237(34)

The molecular conformation can be easily described by splitting both molecules into three parts:

(1) the polyaromatic central cores (atoms C1 to O19 for **A** and C51 to O69 for **B**)
(2) the O—C_8H_{17} alkoxy chains (atoms O35 to C43 for **A** and O85 to C93 for **B**)
(3) the $C^*H(CH_3)$—C_6H_{13} chiral chains (atoms C27 to C34 for **A** and C77 to C84 for **B**).

(1) In the polyaromatic cores, the benzene rings are designated as follows: Φ_{1A} (atoms C1 to C6), Φ_{2A} (atoms C10 to C15), Φ_{3A} (atoms C20 to C25),

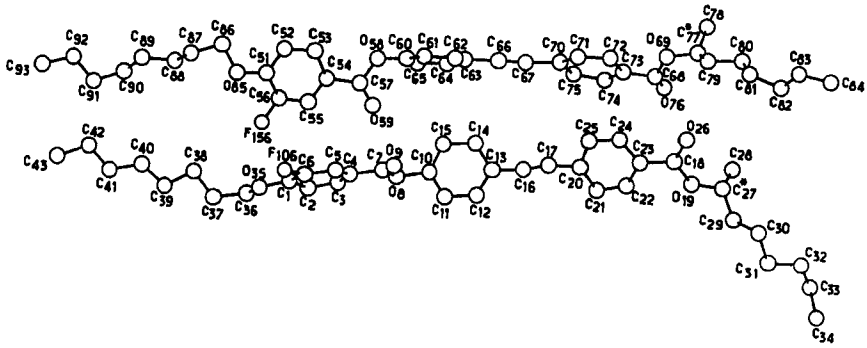

FIGURE 1 Stick-and-ball representation of **A** and **B** molecules of the asymmetric unit of $8FBTO_1M_7$ with atomic labelling.

TABLE III Bond lengths (Å) and standard-deviations in brackets ($\times 10^2$)

	Mole A	*Mole B*		*Mole A*	*Mole B*
C1—C2	1.40 (2)	1.38 (2)	C18—O26	1.22 (1)	1.20 (1)
C1—C6	1.37 (2)	1.36 (2)	O19—C27	1.42 (1)	1.39 (1)
C1—O35	1.40 (1)	1.37 (1)	C20—C21	1.38 (2)	1.39 (2)
C2—C3	1.37 (1)	1.39 (2)	C20—C25	1.36 (2)	1.41 (2)
C3—C4	1.36 (2)	1.40 (2)	C21—C22	1.37 (2)	1.43 (2)
C4—C5	1.36 (2)	1.40 (2)	C22—C23	1.42 (2)	1.41 (2)
C4—C7	1.50 (2)	1.53 (2)	C23—C24	1.41 (2)	1.40 (1)
C5—C6	1.40 (2)	1.36 (2)	C24—C25	1.37 (2)	1.41 (2)
C6—F106	1.35 (1)	1.37 (1)	C27—C28	1.52 (2)	1.53 (2)
C7—O8	1.35 (1)	1.36 (1)	C27—C29	1.49 (2)	1.52 (2)
C7—O9	1.20 (1)	1.21 (1)	C29—C30	1.50 (2)	1.53 (2)
O8—C10	1.37 (1)	1.35 (1)	C30—C31	1.54 (2)	1.51 (2)
C10—C11	1.37 (2)	1.38 (2)	C31—C32	1.50 (3)	1.50 (3)
C10—C15	1.41 (2)	1.37 (2)	C32—C33	1.51 (3)	1.52 (3)
C11—C12	1.43 (2)	1.41 (2)	C33—C34	1.52 (3)	1.51 (3)
C12—C13	1.36 (2)	1.37 (2)	O35—C36	1.44 (2)	1.45 (2)
C13—C14	1.39 (2)	1.36 (2)	C36—C37	1.50 (2)	1.52 (2)
C13—C16	1.43 (2)	1.47 (2)	C37—C38	1.51 (2)	1.52 (2)
C14—C15	1.43 (2)	1.41 (2)	C38—C39	1.55 (2)	1.53 (2)
C16—C17	1.16 (2)	1.17 (2)	C39—C40	1.49 (2)	1.51 (2)
C17—C20	1.45 (2)	1.47 (2)	C40—C41	1.49 (3)	1.50 (3)
C18—O19	1.36 (2)	1.38 (2)	C41—C42	1.47 (3)	1.49 (3)
C18—C23	1.53 (2)	1.53 (2)	C42—C43	1.53 (3)	1.51 (3)

Φ_{1B} (atoms C51 to C56), Φ_{2B} (atoms C60 to C65), Φ_{3B} (atoms C70 to C75).

The two fluorobenzoate groups for both molecules are nearly planar and, respectively for **A** and **B**, are rotated by an angle close to 66° and 65° with the adjacent Φ_2 rings; the Φ_{2A}—C≡C—Φ_{3A} and Φ_{2B}—C≡C—Φ_{3B} tolan groups are only roughly planar, in agreement with the literature [24], the angle between the mean planes being Φ_{3A}/

$\Phi_{2A} = 18°$ and $\Phi_{3B}/\Phi_{2B} = 16°$. The dihedral angle between the tolan groups of molecules **A** and **B** is close to 61°; that between the fluorobenzoate groups of both molecules is close to 58°.

Finally, the polyaromatic central cores for both molecules **A** and **B** are not at all planar and their long axes (C18...O35) and (C68...O85) are almost colinear with an angle close to only 5°. Moreover, molecules **A** and **B** are orientated in the same direction and the polyaromatic core lengths are respectively close to 18.7 and 18.9 Å; the average intercore distance is close to 4.7 Å. The suppress significant torsion angles defining the molecular conformation of molecules **A** and **B** are given in Table IV.

(2) The terminal octyloxy chains OC_8H_{17} are characterized by suppress high thermal motion, probably suggesting some disordered conformations, and are not fully extended with an O—C—C—C torsion angle respectively equal to 69(2)° for **A** and −68(2)° for **B**; their lengths are respectively equal to 9.28(4) and 8.94(3) Å.

(3) The terminal $CH^*(CH_3)—C_6H_{13}$ chiral chains, characterized by some large temperature factors, are not fully extended and have a length close to 7.2 Å for both molecules. Their directions form an angle close to 57° and 38° with the directions of their molecular core, for molecules **A** and **B** respectively. They greatly differ from the angle found in the crystal structures of the well-known antiferroelectric MHPOBC mesogen [10],

TABLE IV Significant* torsion angles (°) of both independent **A** and **B** molecules

Torsion	*Mole A*	*Torsion*	*Mole B*
C5—C4—C7—O8	Trans	C55—C54—C57—O58	166(2)
C4—C7—C8—C10	170(2)	C54—C57—C58—C60	Trans
C7—C8—C10—C11	−60(2)	C57—C58—C60—C61	−104(2)
C24—C23—C18—O19	Trans	C74—C73—C68—O69	158(2)
C23—C18—O19—C27	−157(2)	C73—C68—O69—C77	Trans
C18—O19—C27—C29	158(2)	C68—C69—C77—C79	−125(2)
O19—C27—C29—C30	−153(2)	O69—C77—C79—C80	Trans
C27—C29—C30—C31	Trans	C77—C79—C80—C81	Trans
C29—C30—C31—C32	133(2)	C79—C80—C81—C82	157(2)
C30—C31—C32—C33	−159(3)	C80—C81—C82—C83	124(3)
C31—C32—C33—C34	−93(3)	C81—C82—C83—C84	−168(3)
C1—O35—C36—C37	Trans	C51—O85—C86—C87	Trans
O35—C36—C37—C38	69(2)	O85—C86—C87—C88	−68(2)
C36—C37—C38—C39	Trans	C86—C87—C88—C89	−157(2)
C37—C38—C39—C40	−144(2)	C87—C88—C89—C90	−166(2)
C38—C39—C40—C41	168(2)	C88—C89—C90—C91	154(2)
C39—C40—C41—C42	160(3)	C89—C90—C91—C92	65(3)
C40—C41—C42—C43	Trans	C90—C91—C92—C93	148(2)

* Angles which differ by more than 10° from the trans conformation (180°).

the antiferroelectric $8TBO_1M_7$ [13] and two other antiferroelectric and ferrielectric compounds [11], in which the same chiral chain is perpendicular to the central core.

3.1.2. Molecular Arrangement and Crystal Packing

The projection of the crystal structure on the (**xOz**) plane shows a bilayer arrangement, whose layers are parallel to the (**xOy**) plane.

In two contiguous layers, the molecules have opposite tilt directions ($+11°$ and $-11°$). The molecular arrangement is alternate, smectic A like and is typical of an antiferroelectric arrangement.

The thickness of a layer measured by X-ray diffraction in the S_A phase is equal ot 39.1 Å just above the $K \rightarrow S_A$ melting point. This value is very close to the thickness of a layer in the crystal phase ($c/2$ parameter = 40.3 Å) and also close to the molecular length of 39 Å (when considering the van der Waals radius of the methyl groups ($2^*r(CH_3) = 4$ Å). This suggests that the transition is characterized by a very small reorganization of the molecular arrangement.

Molecular interactions within the sheets are partly due to dipolar interactions between the very polar ether and ester groups, with dipole moments respectively equal to 1.45 and 1.56 Debyes. These dipolar interactions probably maintain the polyaromatic cores of molecules **A** and **B** facing each other.

There are numerous weak van der Waals interactions between neighbouring molecules within the sheet, particularly between the polyaromatic cores.

Interactions between sheets only involve the terminal CH_3 group of the chiral alkyl chains and are due to very weak van der Waals forces.

3.2. Empirical Calculations

3.2.1. Dipolar Moments

The dipolar moment of the $7TBO_1M_7$ molecule is equal to 2.77 D and makes an angle of 37.7° with the long axis of the molecule. This dipole moment vector, whose longitudinal component is preponderant, lies approximately in the benzoate group plane, close to the chiral centre.

It makes an angle of 27° with the tilt plane roughly parallel to the (**xOz**) plane. The carboxylate groups form infinite chains through the head-to-tail molecular arrangement generated by the 2_1 axis parallel to *Oy*, making the

layer highly polar along the **b** axis. Let us recall that the strong polarity in the direction of the normal to the tilt plane was supposed to be responsible for antiferroelectricity [10].

The dipolar moments of the independent molecules **A** and **B** of $8FBTO_1M_7$ are equal to 5.22 and 5.27 D. The global dipolar moment is equal to 4.05 D and makes an angle of 116° with the mean direction of the dimer, while the latter lies approximately in the molecular tilt plane, roughly parallel to the (**xOz**) plane. The global polarization, normal to the tilt plane, is therefore clearly lower than that of $7TBO_1M_7$: indeed, unlike the mesogenic compounds giving birth to the antiferroelectric phasis, the directions of the dipole moments associated with the carboxylate groups are opposing, as suggested by the projection of the structure of $7TBO_1M_7$ on the (**xOz**) plane [13].

This bilayer crystal structure where, by symmetry, the direction of the polarization vector along the **b** axis is alternate from one sheet to another, recalls the established model of the antiferroelectric S^*_{CA} phase.

3.2.2. Binding Energies

Within a sheet, the total binding energy for one molecule of $7TBO_1M_7$ to its six neighbours is −142 kcal *i.e.*, an average between two contiguous molecules of −23.65 kcal, with a large predominance of van der Waals energy. The total binding energy of $8FBTO_1M_7$ "dimer" to its six neighbours within a sheet is equal to −238 kcal, *i.e.*, an average energy of −39.7 kcal per "dimer" with an electrostatic energy contribution of about 25%.

The intersheet energy was evaluated by taking into account three sheets with a limited number* of molecules per sheet, and by calculating the binding energy between the medium sheet on one side and the lower and upper sheets on the other side.

The intersheet energy was found to be about −34.8 kcal for $7TBO_1M_7$ and only −7.1 kcal for $8FBTO_1M_7$, with a large predominance of the van der Waals energy in both compounds. These values are in agreement with the molecular arrangement in the crystal. While $8FBTO_1M_7$ molecules interact only through their terminal methyl groups (see Fig. 2), $7TBO_1M_7$ molecules interact through their whole chiral hexyl groups [13].

* The rigorous evaluation of the intersheet energy should involve a much greater number of molecules in each sheet to limit the effects of series endings. Our calculations already involve a great number of molecules, a very large number of interacting pairs and a long calculation time because of the minimization of the optimal conformation of all molecules.

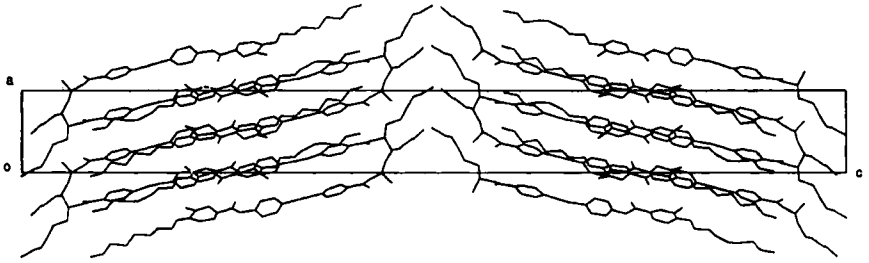

FIGURE 2 Projection of the $8FBTO_1M_7$ structure on the (**xOz**) plane.

4. DISCUSSION

One of the numerous questions is why such a folded conformation is not observed for the $8FBTO_1M_7$ molecule, despite the presence of a chiral alkyl chain identical to that of the $7TBO_1M_7$ molecule, and why this feature seems to be related to antiferroelectricity.

This could be due to the completely different molecular arrangement, which is determined by the relative positions of the ester and ether groups in the polyaromatic cores.

In a recent paper, Hori and Ohashi [3] proposed a model for the molecular arrangement and intermolecular O...O (ester and ether groups) interactions, revealed by the crystal structures of a few chiral smectogenic biphenyl esters. They asserted that the intermolecular interactions, constructing layer structures, can be divided into two factors: overlapping of molecules and interactions between ether and ester polar groups. They proposed two modes of possible arrangement, in relation to the length of the core molecular fragment between the latter groups:

- Only the ester groups are associated with each other, with an antiparallel arrangement between interacting molecules (mode I, Fig. 3).
- The ester and ether groups are close at two positions between neighbouring molecules (mode II, Fig. 3).

According to Hori and Ohashi [3], the molecular arrangement in $8FBTO_1M_7$ and $7TBO_1M_7$ crystal structures is probably induced by electrostatic interactions between the polar groups. This is obviously the case for $7TBO_1M_7$, whose molecular arrangement belongs to the mode II type [13], with interactions between ester and ether groups on both ends of the tolan group (Fig. 4a).

As far as $8FBTO_1M_7$ molecular arrangement is concerned, there are dipolar interactions between the ester groups located on both sides of the

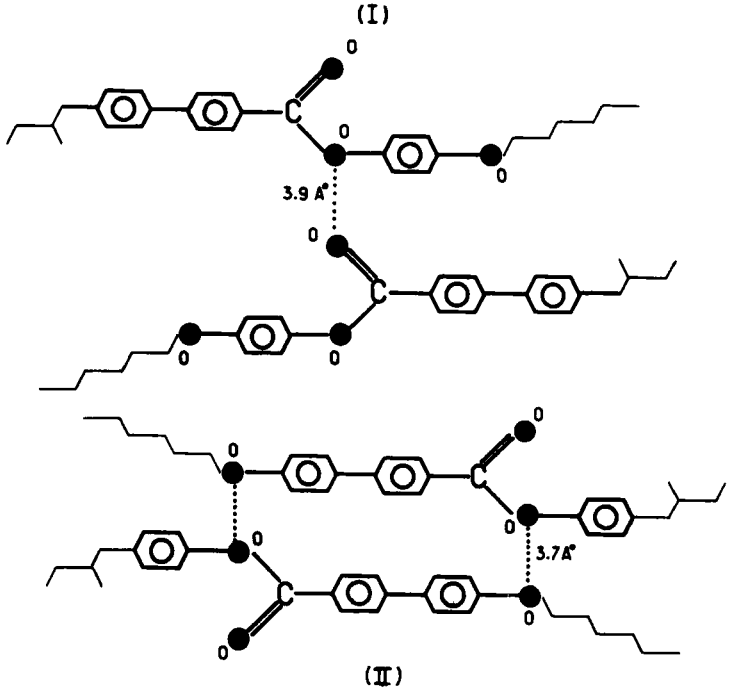

FIGURE 3 Modes of arrangement of polyaromatic cores according to Hori and Ohashi [3].

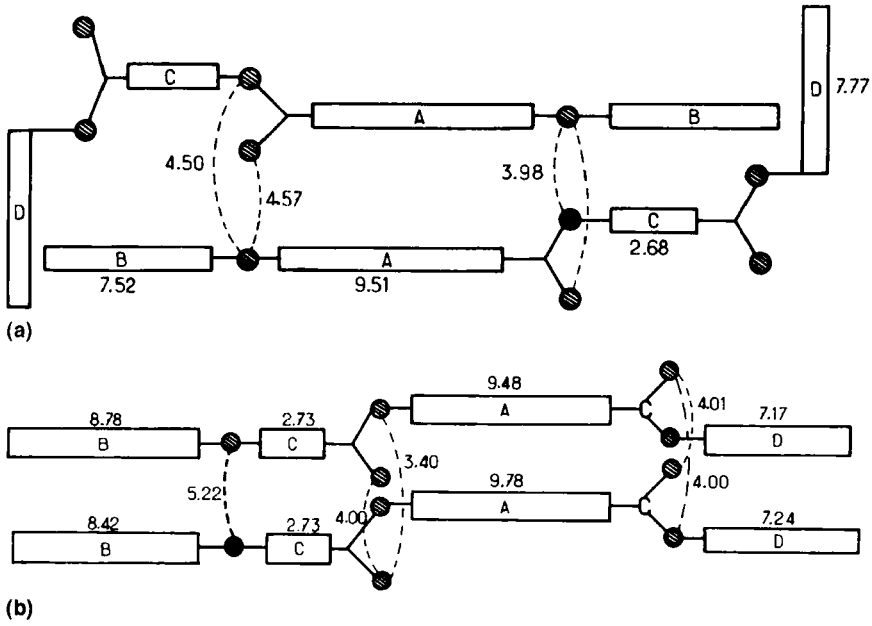

FIGURE 4 Schematic molecular arrangement of $7TBO_1M_7$ (a) and $8FBTO_1M_7$ (b).

tolan group, on the one hand, and between ether groups of the alkoxy chains, on the other. This arrangement does not belong to mode II but could be related in some way to mode I (Fig. 4b).

Anyway, the interesting feature is that in both $8FBTO_1M_7$ and $7TBO_1M_7$ crystal structures, the tolan groups are facing each other with numerous van der Waals interactions. Let us assume that the face-to-face arrangement of the tolan groups in contiguous molecules is a prime necessity for the molecular arrangement.

In the $8FBTO_1M_7$ crystal structure, the fact that molecules **A** and **B** have the same orientation (Fig. 4b) results in a maximum overlap of their polyaromatic central core and alkoxy chain, but also prevents the chiral hexyl chains from being perpendicular to the cores. Therefore, they are in the prolongation of these cores. As a result, the alkoxy chains, on the one hand, and the chiral hexyl chains, on the other, are facing each other. However, if molecules **A** and **B** were antiparallel, there would no longer be an overlap of their central core and the alkoxy chain and the molecules would be unable to give rise to sheets.

On the contrary, in the $7TBO_1M_7$ crystal structure, where contiguous molecules are antiparallel (Fig. 4a), there is an overlap between the moieties including the polyaromatic central core and the alkoxy chains, and particularly between the adjacent tolan groups. Moreover, the chiral hexyl chains are perpendicular to the core, so they can give rise to sheets (Fig. 5). This arrangement is similar to that observed in the MHPOBC crystal structure [10].

If we now suppose that the contiguous molecules have the same orientation, nothing can prevent them from displaying a large overlap as is the case for $8FBTO_1M_7$. However, a head-to-tail arrangement is more probable, as far as the dipole–dipole interactions are concerned.

Finally, according to our hypothesis, if the configuration in which the tolan groups of contiguous molecules are facing each other is probable, the folding of the chiral hexyl chain would depend on the distance between the tolan group and the chiral chain. If this distance is too short, as is the case for $8FBTO_1M_7$, such a folding is not probable.

Up to now, the existence of a antiferroelectric phase for MHPOBC [10], some of its derivatives [11, 12] and $7TBO_1M_7$ [13], showing the CO_2—Ø—CO_2—$C^*H(CH_3)$—C_6H_{13} chaining, has been related to their crystal structure, characterized by a chiral alkyl chain perpendicular to the polyaromatic central core. This conformation is the one that minimizes the distance between the transverse dipole located in the proximity of the chiral centre for two molecules strongly interacting through their chains.

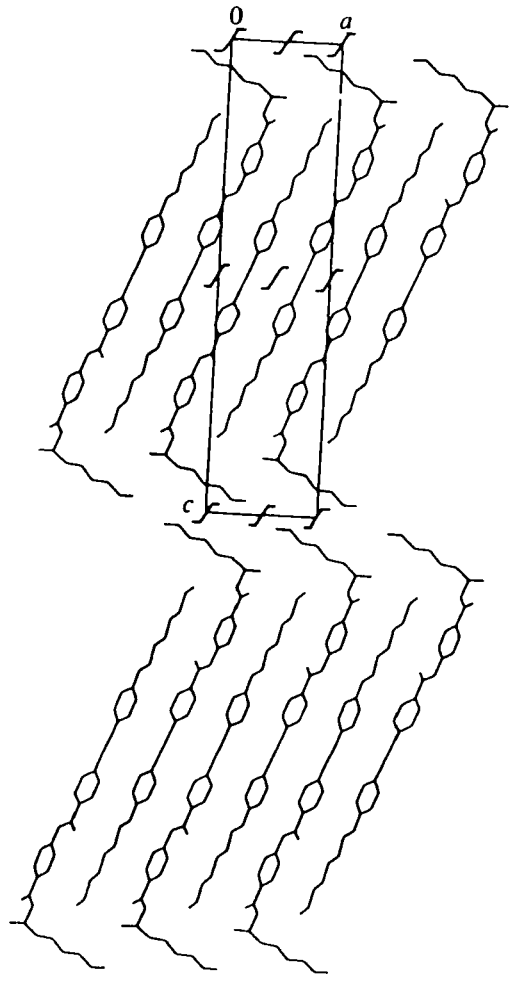

FIGURE 5 Projection of the $7TBO_1M_7$ structure on the (**xOz**) plane [13].

Such a conformation does not exist for $8FBTO_1M_7$, for which only the S_A phase is present.

References

[1] P. Kromm, J. P. Bideau, M. Cotrait, C. Destrade and H. T. Nguyen, *Acta Cryst.*, **C50**, 441 (1994).
[2] P. Kromm, H. Allouchi, J. P. Bideau and M. Cotrait, *Mol. Cryst. Liq. Cryst.*, **257**, 9 (1994).
[3] K. Hori and Y. Ohashi, *Mol. Cryst. Liq. Cryst.*, **203**, 171 (1991).

[4] K. Hori and Y. Ohashi, *Bull. Soc. Chem. Jpn.*, **61**, 3859 (1988).
[5] K. Hori, M. Takamatsu and Y. Ohashi, *Bull. Chem. Soc. Jpn.*, **62**, 1751 (1989).
[6] K. Hori and Y. Ohashi, *J. Mater. Chem.*, **1**(4), 667 (1991).
[7] K. Hori and Y. Ohashi, *Bull. Chem. Soc. Jpn.*, **62**, 3216 (1989).
[8] I. Zareba, H. Allouchi, M. Cotrait, M. F. Narbor, H. T. Nguyen and C. Destrade, *Ferroelectrics*, **180**, 117 (1996).
[9] I. Zareba, H. Allouchi, M. Cotrait, M. F. Narbor, C. Destrade and H. T. Nguyen, *Liq. Crystals*, **21**(4), 565 (1996).
[10] K. Hori and K. Endo, *Bull. Chem. Soc. Jpn.*, **66**, 46 (1993).
[11] K. Hori, S. Kawahara and K. Ito, *Ferroelectrics*, **147**, 91 (1993).
[12] K. Hori, M. Takamatsu and Y. Ohashi, *Ferroelectrics*, **85**, 485 (1988).
[13] I. Zareba, H. Allouchi, M. Cotrait, C. Destrade and H. T. Nguyen, *Acta Cryst.*, **C52**, 441 (1996).
[14] G. W. Gray and J. W. Goodby, Smectic Liquid Crystals, Leonard Hill, Glasgow (1984).
[15] H. T. Nguyen, R. J. Twieg, M. F. Narbor, N. Isaert and C. Destrade, *Ferroelectrics*, **121**, 187 (1991).
[16] P. Cluzeau, H. T. Nguyen, C. Destrade, N. Isaert, P. Barois and A. Babeau, *Mol. Cryst. Liq. Cryst.*, **260**, 69 (1995).
[17] A. C. T. North, D. C. Phillips and F. S. Matthews, *Acta Cryst.*, **A24**, 351 (1968).
[18] C. J. Gilmore, *J. Appl. Cryst.*, **17**, 42 (1984).
[19] G. M. Sheldrick, Shelx86, Program for the Solution of Crystal Structures, Univ. of Göttingen, Germany (1986).
[20] G. M. Sheldrick, Shelx76, Program for Crystal Structure Determination, Univ. of Cambridge, England (1976).
[21] P. Dauber-Osguthorpe, V. A. Roberts, D. J. Osguthorpe, J. Wolff, M. Genest and A. T. Hagler, Structure and energetics of ligand to proteins: structure function and genetics.
[22] H. Allouchi, J. P. Bideau, M. Cotrait, C. Destrade and H. T. Nguyen, *Mol. Cryst. Liq. Cryst.*, **239**, 153 (1994).
[23] H. Allouchi, M. Cotrait, D. Guillon, B. Heinrich and H. T. Nguyen, *Chem. Materials*, **7**, 2252 (1995).
[24] M. Cotrait, C. Destrade and H. Gasparoux, *Mol. Cryst. Liq. Cryst.*, **39**, 159 (1977).